PERGAMON

Journal of Quantitative Spectroscopy & Radiative Transfer 77 (2003) 395–416

Journal of Quantitative Spectroscopy & Radiative Transfer

www.elsevier.com/locate/jqsrt

Stochastic radiative transfer in multilayer broken clouds. Part II: validation tests

Evgueni Kassianov*, Thomas Ackerman, Roger Marchand, Mikhail Ovtchinnikov

Pacific Northwest National Laboratory, 902 Battelle Boulevard, P.O. Box 999, Richland, WA 99352, USA

Received 25 March 2002; accepted 10 July 2002

Abstract

In the second part of our two-part paper, we estimated the accuracy and robustness of the approximated equations for the mean radiance that were derived in Part I. In our analysis we used the three-dimensional (3D) cloud fields provided by (i) the stochastic Boolean model, (ii) large-eddy simulation model and (iii) satellite cloud retrieval. The accuracy of the obtained equations was evaluated by comparing the *ensemble-averaged* radiative properties that were obtained by the numerical averaging method (reference) and the analytical averaging method (approximation). The robustness of these equations was estimated by comparing the *domain-averaged* radiative properties obtained by using (i) the full 3D cloud structure (reference) and (ii) the bulk cloud statistics (approximation). It was shown that the approximated equations could provide reasonable accuracy (~15%) for both the ensemble- and domain-averaged radiative properties.

Keywords: Overlapping broken clouds; Solar radiation; Stochastic approach

1. Introduction

Real three-dimensional (3D) broken clouds may have extreme inhomogeneity in both horizontal and vertical directions. The cloud variability determines the radiation variations. Since the cloud variability occurs over large spatial/temporal scales, it is important to get answers for the following two questions: What cloud statistics are needed to calculate the mean radiative properties accurately? How can these statistics be incorporated into radiative calculations? A few analyses have been performed for a *single* cloud layer, to determine the most significant statistics of cloud fluctuations that determine the mean radiative properties (see e.g. [1,2]). In particular, it was demonstrated that the mean radiative fluxes are not sensitive to the details of these statistics. For calculating

* Corresponding author. Tel.: +1-509-372-6535; fax: +1-509-372-6168.
E-mail address: evgueni.kassianov@pnl.gov (E. Kassianov).

0022-4073/03/$ - see front matter
PII: S0022-4073(02)00171-1

the mean radiative properties of *multilayer* inhomogeneous clouds, one has to describe both the variability in each cloud layer and the statistical relationship between layers [3]. Currently, most theoretical methods for treating overlap of fractional clouds are limited by the maximum-random overlap assumptions [4]: two adjacent cloud layers are maximally overlapped, and the random overlap only happens for separated layers.

An approach for the stochastic description of the solar radiation transfer through broken fields with the arbitrary horizontal and vertical inhomogeneity was introduced in the first part of our paper [5] (hereafter referred to as Part I). Different combinations of the random and maximum cloud overlap can be treated by the suggested approach. We derived the approximated equations for both the mean direct and diffuse solar radiance on the basis of the stochastic transfer equation and a new statistically inhomogeneous Markovian model of broken clouds (Part I).

The purpose of this paper is to estimate the accuracy and robustness of the approximated equations by using the 3D broken cloud fields that were (i) produced by the Boolean stochastic model, (ii) simulated by a large-eddy simulation (LES) model and (iii) derived from collocated and coincident multi-angle imaging spectroradiometer (MISR) and ground-based observations. An outline of the Markovian approach is described in Section 2. In Section 3, we introduce different cloud fields of broken clouds that have been used in our validation analysis. The results of the radiative calculations and their analysis are presented in Section 4. The conclusion is provided in Section 5.

2. Markovian approach

In this section, an overview of the suggested approach (Part I) is given. The irregular geometry of broken clouds has been described by unconditional $\langle\kappa(\mathbf{r})\rangle = P\{\kappa(\mathbf{r}) = 1\}$ and conditional $V(\mathbf{r}_2, \mathbf{r}_1) = P\{\kappa(\mathbf{r}_2) = 1 \mid \kappa(\mathbf{r}_1) = 1\}$ probabilities of the cloud presence (Markovian assumption). Here $\mathbf{r} = (x, y, z)$ is a vector to a point in space and $\kappa(\mathbf{r})$ is the random indicator field, $\kappa(\mathbf{r}) = 1$ inside clouds, and $\kappa(\mathbf{r}) = 0$ outside clouds. The angular brackets will be used for ensemble averages over $\kappa(\mathbf{r})$. A new statistically inhomogeneous Markovian model has been suggested to describe both the horizontal and vertical variability of broken clouds. The term "statistical inhomogeneity" is understood to mean that the unconditional probability (or cloud fraction) $\langle\kappa(\mathbf{r})\rangle$ depends on the vertical coordinate and the conditional probability $V(\mathbf{r}_2, \mathbf{r}_1)$ depends on the mutual arrangement of the points $\mathbf{r}_2$ and $\mathbf{r}_1$. As an illustration, some examples are given below

if the point $\mathbf{r}_1 = (x_1, y_1, z_1)$ and $\mathbf{r}_2 = (x_2, y_2, z_1)$ belong to the same kth layer, then

$$V_k(\mathbf{r}_2, \mathbf{r}_1) = (1 - p_k) \times \exp(-A_k \times |\mathbf{r}_2 - \mathbf{r}_1|) + p_k, \tag{1}$$

where p_k is cloud fraction in the kth layer, and A_k is parameter;

if the point $\mathbf{r}_1 = (x_1, y_1, z_1)$ and $\mathbf{r}_2 = (x_1, y_1, z_2)$ belong to different *adjacent* layers, namely kth and mth layers, then

$$V_{k,m}(\mathbf{r}_2, \mathbf{r}_1) = \exp(-A^* \times |\mathbf{r}_* - \mathbf{r}_2|) \times \{V_k(\mathbf{r}_1, \mathbf{r}_*) - p_m\} + p_m, \tag{2}$$

where $\mathbf{r}_* = \mathbf{r}_1 + \boldsymbol{\omega} \times (z_* - z_1)/c$, $\boldsymbol{\omega} = (a, b, c) = (\mathbf{r}_2 - \mathbf{r}_1)/|\mathbf{r}_2 - \mathbf{r}_1|$.

For the upward direction ($c > 0$), $m = k + 1$, $A^* = A_k^{\mathrm{up}}$ and z_* equals the top altitude of the kth layer, $z_* = z_k$; for the downward direction ($c < 0$), $m = k - 1$, $A^* = A_k^{\mathrm{dw}}$ and z_* equals the

base altitude of the kth layer, $z_* = z_{k-1}$. Parameters A_k^{up} and A_k^{dw} determine the statistical relationship between kth layer and its upper $(k+1)$ and lower $(k-1)$ adjacent layers, respectively. Note, all these parameters A_k, A_k^{up} and A_k^{dw} depend on both the 3D cloud structure and the positions of points $\mathbf{r}_1$ and $\mathbf{r}_2$. By changing the values of these parameters, one can describe different combinations of maximum and random cloud overlaps. This sketched flexibility of the inhomogeneous model is its appealing feature.

The statistically inhomogeneous model of broken clouds and the stochastic transfer equation were used to derive approximated equations for the mean solar radiance (Part I). It was assumed that for each kth layer the domain-averaged optical properties are constant (piecewise constant approximation), e.g., the extinction coefficient $\sigma(\mathbf{r}) = \sigma(z) = \sigma_k$, the single scattering albedo $\omega_0(\mathbf{r}) = \omega_0(z) = \omega_{0,k}$ and the scattering phase function $g(\mathbf{r}, \boldsymbol{\omega}, \boldsymbol{\omega}') = g(z, \boldsymbol{\omega}, \boldsymbol{\omega}') = g_k(\boldsymbol{\omega}, \boldsymbol{\omega}')$. Also it was assumed that a parallel unit flux of solar radiation is incident on the upper boundary of a given cloud field in direction $\boldsymbol{\omega}_\oplus$. To get the absolute values one should multiply the calculated radiative properties by the spectral solar constant weighted with $\cos(\xi_\oplus)$, where $\xi_\oplus$ is the solar zenith angle (SZA). The equations were obtained without considering the aerosol-molecular atmosphere and underlying surface; the latter can be added quite easily.

The equation for the mean solar radiance has the form

$$\langle I(z, \boldsymbol{\omega}) \rangle = \frac{1}{|c|} \int_{E_z} \omega_0(\xi) \phi(z, \xi) \, \mathrm{d}\xi \int_{4\pi} g(\xi, \boldsymbol{\omega}, \boldsymbol{\omega}') f(\xi, \boldsymbol{\omega}') \, \mathrm{d}\boldsymbol{\omega}' + \langle j(z, \boldsymbol{\omega}) \rangle \delta(\boldsymbol{\omega} - \boldsymbol{\omega}_\oplus), \tag{3}$$

where $E_z = (h_\mathrm{b}, z)$ if $c > 0$, and $E_z = (z, h_\mathrm{t})$ if $c < 0$, h_t and h_b are the top height and the base height of cloud field, respectively; $\langle j(z, \boldsymbol{\omega}) \rangle$ is the mean direct (unscattered) radiance, and $f(z, \boldsymbol{\omega}) = \sigma(\mathbf{r}) \langle \kappa(\mathbf{r}) I(\mathbf{r}, \boldsymbol{\omega}) \rangle$ is the mean collision density, $\delta(\cdot)$ is Dirac's delta function.

An integral equation for the mean collision density can be written as

$$f(\mathbf{x}) = \int_X k(\mathbf{x}, \mathbf{x}') f(\mathbf{x}') \, \mathrm{d}\mathbf{x}' + \Psi(\mathbf{x}), \tag{4}$$

$$k(\mathbf{x}, \mathbf{x}') = \frac{\omega_0(z) g(z, \boldsymbol{\omega}, \boldsymbol{\omega}') \eta(\mathbf{r}, \mathbf{r}')}{2\pi |\mathbf{r} - \mathbf{r}'|^2} \, \delta\left(\frac{\mathbf{r} - \mathbf{r}'}{|\mathbf{r} - \mathbf{r}'|} - \boldsymbol{\omega} \right), \tag{5}$$

$$\Psi(\mathbf{x}) = \sigma(z) p(z) v(z, \boldsymbol{\omega}) \delta(\boldsymbol{\omega} - \boldsymbol{\omega}_\oplus), \tag{6}$$

where X is the phase space of coordinates and directions, $\mathbf{x} = (\mathbf{r}, \boldsymbol{\omega})$. All functions $\phi(\mathbf{r}, \mathbf{r}'), \eta(\mathbf{r}, \mathbf{r}')$ and $v(z, \boldsymbol{\omega}) = \langle \kappa(\mathbf{r}) j(\mathbf{r}, \boldsymbol{\omega}) \rangle / p(z)$ are defined by the recurrent expressions (Part I).

The closed system of equations (3)–(4) can be solved by using any appropriate numerical methods or analytic techniques (e.g., the spherical harmonic method). Here, to solve these approximated equations, we apply the Monte Carlo method. The latter is based on simulating a Markovian chain (e.g. [6]). In particular, we used the method of direct simulation to calculate the absorption and radiative fluxes. In this simulation technique, the photon trajectory modeling was made in correspondence with the initial $\Psi(\mathbf{x})$ and transitional $k(\mathbf{x}, \mathbf{x}')/\omega_0(z)$ densities of integral equation (4), while the radiative properties were estimated in accordance with their physical contents [6]. For instance, the upward flux $F_{\mathrm{up}}(z_i)$ at the altitude $z = z_i$ was estimated from the mean number of photon crossings of

the plane $z = z_i$ in directions satisfying the inequality $c > 0$. Hereafter, we will use subscripts, "up", and, "dw", for upward and downward radiation, respectively. In addition, the method of direct simulation was used to calculate (i) the histograms of photon path length distributions in the transmitted $J_{\mathrm{dw}}(l)$ and reflected $J_{\mathrm{up}}(l)$ radiation and (ii) the angular distribution histograms of the transmitted $f_{\mathrm{dw}}(\vartheta)$ and reflected $f_{\mathrm{up}}(\vartheta)$ radiation. Here

$$\int_0^\infty J_{\mathrm{dw}}(l)\,\mathrm{d}l = \langle T_{\mathrm{d}}\rangle, \quad \int_0^\infty J_{\mathrm{up}}(l)\,\mathrm{d}l = \langle R\rangle, \tag{7}$$

where l is the photon path length, $\langle T_{\mathrm{d}}\rangle$ and $\langle R\rangle$ are the mean diffuse transmittance (at the cloud base) and the mean albedo (at the cloud top), respectively:

$$f_{\mathrm{up(dw)}}(\vartheta_{i+1}) = \frac{1}{2\pi(\vartheta_i - \vartheta_{i+1})}\int_0^{2\pi}\mathrm{d}\varphi\int_{\vartheta_i}^{\vartheta_{i+1}}\langle I_{\mathrm{up(dw)}}(\vartheta,\varphi)\rangle\,\mathrm{d}\vartheta, \tag{8}$$

where $\vartheta_i = i \times 10,\ i = 0,\ldots,9$; $\langle I_{\mathrm{up(dw)}}(\vartheta,\varphi)\rangle$ is the mean radiance of reflected and transmitted radiation at the cloud top ($z = h_{\mathrm{t}}$) and the cloud base ($z = h_{\mathrm{b}}$), respectively; ξ and φ are the zenith and azimuth angles and $\vartheta = \cos\xi$.

As was described in Part I, the statistically inhomogeneous model has relatively few input parameters, which describe only the bulk *geometrical* statistics of the 3D broken cloud field. Thus, the question arises: how accurately can equations derived on the basis of the statistically inhomogeneous model represent the mean *radiative* properties (e.g., mean fluxes, mean absorption) of the 3D broken cloud fields? To answer this question, the following will be done for different 3D cloud fields. First, we obtain the mean radiative properties exactly by applying 3D radiative transfer calculations directly to a given full 3D cloud structure. The obtained radiative properties will be considered as a reference. Second, for a given 3D cloud field, we calculate the *bulk* cloud statistics, that will be served as input data for the statistically inhomogeneous model. Next, we estimate the mean radiative properties by applying the approximated equations (3), (4). The obtained radiative properties will be considered as approximations of true ones. Finally, we will compare the mean radiative properties obtained by using the independent exact method (references) with ones obtained for the statistically inhomogeneous model (approximations).

3. Cloud fields

In our analysis, we used three different fields of 3D broken clouds, which represent marine low-level cumulus clouds (Fig. 1). For each of these fields, the bulk geometrical statistics have were derived and then used as input data to calculate the mean radiative properties (next section).

Boolean cloud fields: An ensemble of cloud realizations (Figs. 1a,d) was obtained by using a Boolean stochastic model (e.g. [7]). Note, Boolean models can be considered as fundamental models for the stochastic geometry and allows one to easily obtain an *ensemble* of cloud field realizations (samples) with given mean geometrical properties (e.g., cloud fraction, horizontal D and vertical H sizes) and different vertical structure. In our simulations, the values of these parameters were matched to the typical values for marine low-level cumulus clouds. Below, we use the term "Boolean cloud field(s)" as a reference to cloud field(s) generated by the Boolean model.

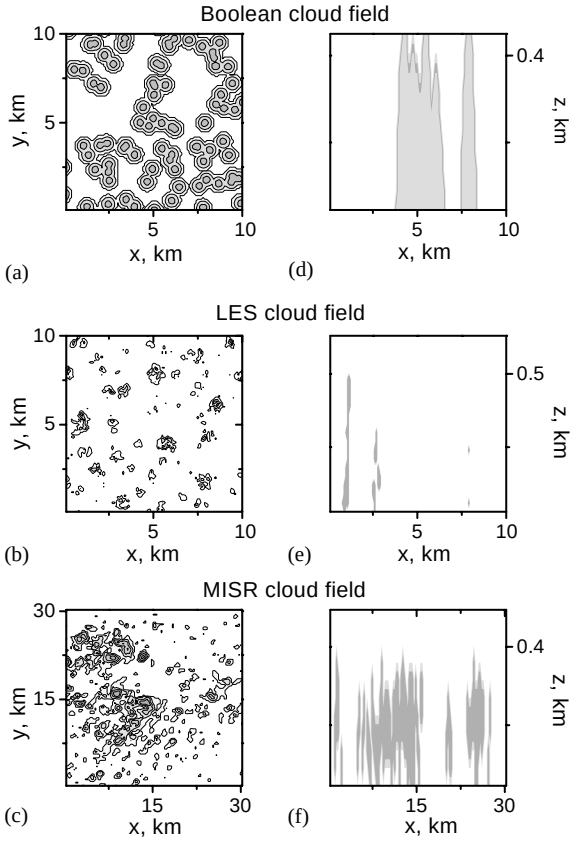

Fig. 1. The horizontal (left column) and the vertical (right column) distributions of broken clouds that are provided by the Boolean stochastic model (a,d), LES model (b,e) and MISR cloud retrieval (c,f). The vertical cross-sections corresponding to $y = yl/2$, where yl is domain size in y-direction. Brightness in the horizontal distributions (left column) is proportional to the geometrical thickness of clouds.

LES cloud field: The second field of marine low-level cumulus clouds (single realization) was provided by the LES model (Figs. 1b,e). Data from the Atmospheric Radiation Measurement Program's (ARM) Tropical Western Pacific (TWP) site was used to initialize the LES model. The cloud field was simulated in domain $10 \times 10 \times 2\ \mathrm{km}^3$ with 0.1 km horizontal and 0.033 km vertical resolution. The simulated 3D cloud field is highly variable in both horizontal and vertical dimensions. For example, height of cloud base above lifting condensation level varies in the interval from 0.1 to 0.6 km, while its mean value is equal to 0.2 km. Below we use the term "LES cloud field" to represent cloud field derived from LES simulations.

MISR cloud field: The third field of marine low-level cumulus clouds (single realization) was obtained from collocated and coincident MISR and ground-based radar observations in the tropical Pacific region at the island of Nauru [8]. The reconstructed 3D geometry of broken clouds (Figs. 1c,f) corresponds to the domain $\sim 30 \times 30 \times 2\ \mathrm{km}^3$ with 0.275 km horizontal resolution (total number of pixels is 110×110). Cloud top/base heights were provided for the z-direction. Below, we will use the term "MISR cloud field", which corresponds to cloud field derived from MISR retrieval.

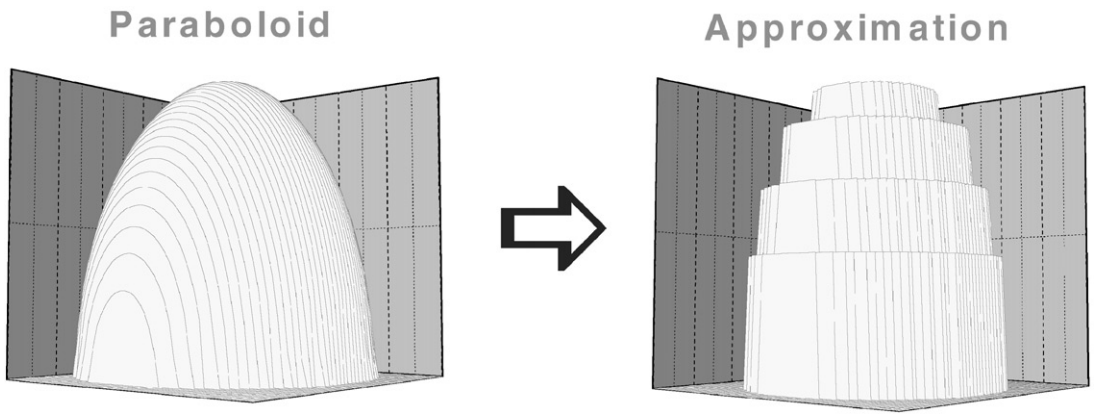

Fig. 2. Schematic diagram illustrates the approximation of a truncated paraboloid of revolution by a set of cylinders with different diameters.

3.1. Simulations of Boolean fields

The Boolean cloud fields were used to estimate an accuracy of approximated equations (3), (4). The latter were obtained for Markovian cloud fields (Part I). To estimate the accuracy correctly, we simulated Markovian cloud fields. In particular, the spatial Poisson process was simulated by using the Boolean model (e.g. [7]). There are two basic steps in constructing 3D cloud samples by using a Boolean model: (a) simulations of a number of cloud centers and their distribution in space/plane and (b) simulations of a sequence of clouds with given geometrical form (e.g., spheres, cylinders, etc.). The individual clouds may intersect, forming more complex configurations. We assume that broken clouds occupy a certain region in space (simulation domain) in the form of parallelepiped with thickness H, the base of which is a square with sides xl. In our simulations, the 3D cloud fields (cloud realization) were formed by a group of truncated paraboloids of revolution with fixed diameter D and height H (aspect ratio $\gamma = H/D$). These parameters are set to values typical for small marine cumulus clouds (e.g. [9]). The simulations were performed for different nadir-view cloud fractions N_{nadir} (the horizontal area fraction covered by clouds as viewed from nadir). The centers of the individual clouds, which we assume are the geometrical centers of the figures, are arranged randomly on the horizontal plane $z = hb$. We divided the domain into $100 \times 100 \times 10$ identical pixels. Each pixel has the same horizontal $\Delta x = \Delta y = 0.1$ km ($xl = 10$ km) and vertical $\Delta z = 0.045$ km sizes. The latter was chosen to correspond to the vertical resolution of radar observations (e.g. [10]). Then the value of indicator field $\kappa(\mathbf{r})$ is determined for each pixel (i, j, k) as a value of $\kappa(\mathbf{r})$ at a point $\mathbf{r}^* = (x_i, y_i, z_k)$, where $x_i = i\,\Delta x$, $y_j = j\,\Delta y$, $z_k = k\,\Delta z$, $i = 1, \ldots, 100$, $j = 1, \ldots, 100$, $k = 1, \ldots, 10$. Pixel (i, j, k) is considered as a cloudy pixel if $\kappa(\mathbf{r}^*) = 1$ (point $\mathbf{r}^*$ belongs to the cloud). The reverse is true if $\kappa(\mathbf{r}^*) = 0$ (point $\mathbf{r}^*$ does not belong to the cloud). As a result of this discretization, the geometrical shape of an individual cloud (truncated paraboloid of revolution) is approximated by a set of cylinders (Fig. 2) with the same height $\Delta h = H/10$ and different diameters D. Note, the centers of these cylinders have the same horizontal coordinates, and therefore correspond to the maximum overlap assumption. To get random cloud overlap, for each

layer one should distribute the centers of these cylinders randomly and independently on a horizontal plane.

3.2. Bulk cloud statistics

Here, we outline an approach for deriving bulk geometrical statistics of 3D broken clouds. The conditional probability may have a rather complex dependence on points $\mathbf{r}_1$, $\mathbf{r}_2$, and 3D cloud structure. Indeed, in the general case, the probability that the indicator function $\kappa(\mathbf{r}_2)$ is assigned the value 1 (point $\mathbf{r}_2$ belongs to cloud) depends on the values of $\kappa(\mathbf{r})$ at all other points, that belong to a given cloud field. Because of this, deriving simple analytical functions is problematic. To avoid this difficulty, it is possible to simplify this dependence, for example, by assuming that the value of the indicator function $\kappa(\mathbf{r}_2)$ depends only on the knowledge of the $\kappa(\mathbf{r})$ values at *neighboring* pixels (Markovian approximation). Note, that the Markovian approximation was used to derive simple analytical formulas for the conditional probabilities (see Eqs. (1) and (2)). Here, we define the neighboring pixels as pixels with a common edge or vertex.

There are a few basic steps for deriving bulk geometrical statistics for a given 3D cloud field. First, we calculate the cloud fraction (the unconditional probability of cloud presence) for each layer of the 3D cloud field. Second, we compute the conditional probabilities of cloud presence for each kth layer in both the x- and y-directions. Third, we determine the conditional probabilities of cloud presence for two adjacent layers in both the upward and downward directions. Finally, we derive parameters $A_{k,x}$ (x-direction), $A_{k,y}$ (y-direction) and A_k^{up}, A_k^{dw} (upward and downward directions) for each kth layer by using obtained probabilities and Eqs. (1) and (2). For example, from Eq. (1) it follows, that parameter $A_{k,x}$ can be estimated as

$$A_{k,x} = -\ln\left(\frac{V_k(\mathbf{r}_2,\mathbf{r}_1) - p_k}{1 - p_k}\right)\Big/|\mathbf{r}_2 - \mathbf{r}_1|, \tag{9}$$

where $|\mathbf{r}_2 - \mathbf{r}_1| = \Delta x$; p_k and $V_k(\mathbf{r}_2,\mathbf{r}_1)$ are the unconditional and conditional probabilities of cloud presence, respectively. These probabilities have been obtained numerically from a given 3D cloud field. In a similar way, $A_{k,y}$ can be calculated. The parameter A_k was approximated as $A_k = A_{k,x}|a| + A_{k,y}|b|$.

As another example, we write equation for A_k^{dw} (the nadir direction). From Eqs. (1) and (2) and $A_k = 0$, it follows that

$$A_k^{\mathrm{dw}} = -\ln\left(\frac{V_{k,k-1}(\mathbf{r}_2,\mathbf{r}_1) - p_{k-1}}{1 - p_{k-1}}\right)\Big/|\mathbf{r}_2 - \mathbf{r}_1|, \tag{10}$$

where $|\mathbf{r}_2 - \mathbf{r}_1| = \Delta z$; p_k and $V_{k,k-1}(\mathbf{r}_2,\mathbf{r}_1)$ are the unconditional and conditional probabilities of cloud presence, respectively. These probabilities have been derived from a given 3D cloud field. If two adjacent cloud layers, namely kth and $(k-1)$th layers, are perfectly dependent (maximum cloud overlap), then $V_{k,k-1}(\mathbf{r}_2,\mathbf{r}_1) = 1$ and $A_k^{\mathrm{dw}} = 0$. If these two adjacent cloud layers are perfectly independent (random cloud overlap), then $V_{k,k-1}(\mathbf{r}_2,\mathbf{r}_1) = p_{k-1}$ and $A_k^{\mathrm{dw}} \gg 1$. In a similar way, parameters A_k^{dw} and A_k^{up} can be calculated for different positions of points $\mathbf{r}_1$ and $\mathbf{r}_2$. Note, that for statistically

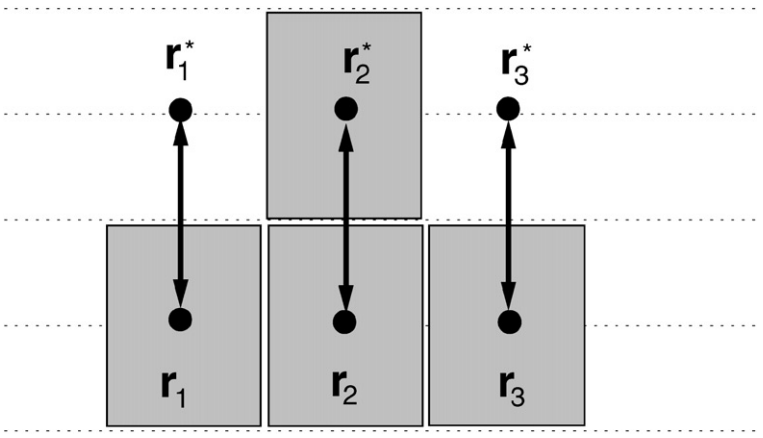

Fig. 3. Schematic diagram illustrates the differences of the cloud overlap in upward and downward directions. Upper layer contains only one cloud pixel. Bottom layer has three cloud pixels. Here we consider the upward (zenith) and downward (nadir) directions only. If point $\mathbf{r}$ belongs to a cloud pixel in the upper layer, then it belongs to a cloud pixel in the bottom layer (points $\mathbf{r}_2^*$ and $\mathbf{r}_2$). The reverse cannot be valid (points $\mathbf{r}_1$ and $\mathbf{r}_1^*$; and points $\mathbf{r}_1$ and $\mathbf{r}_1^*$).

inhomogeneous fields ($p_k \neq p_{k-1}$), the following inequality is valid (Part I)

$$V_{k,k-1}(\mathbf{r}_2, \mathbf{r}_1) \neq V_{k-1,k}(\mathbf{r}_1, \mathbf{r}_2). \tag{11}$$

In other words, two adjacent cloud layers, namely kth and $(k-1)$th layers, can be *perfectly* dependent in the downward direction ($V_{k,k-1}(\mathbf{r}_2, \mathbf{r}_1) = 1$), but can have another statistical relationship (different from perfect) in the upward direction ($V_{k-1,k}(\mathbf{r}_1, \mathbf{r}_2) < 1$). The following schematic diagram illustrates this possible situation (Fig. 3).

The cloud statistics can be calculated from the single cloud realization (domain-averaged values) or from an ensemble of cloud realizations (ensemble-averaged values). For both the MISR cloud field and the LES cloud field, only domain-averaged cloud statistics were derived from corresponding single cloud realizations. For the Boolean model, the ensemble-averaged cloud statistics were obtained (averaging over 10000 realizations). We performed simulations of the Boolean cloud fields and corresponding radiative calculations for a set of cloud geometrical parameters, but here we present results for mean cloud diameter $D = 1$ km, cloud height $H = 0.5$ km (aspect ratio $\gamma = 0.5$), and the nadir-view cloud fraction $N_{\text{nadir}} = 0.5$.

The numerical experiments with other cloud geometrical parameters provide similar results (accuracy of approximated equations), which are discussed below. The examples of the bulk cloud statistics are presented in Fig. 4. It is easily seen that vertical profiles of cloud fraction and mean cloud horizontal size (chord) may have both large quantitative and qualitative differences for the considered cloud fields (Fig. 1). Since cloud statistics are almost identical for both x- and y-directions, here we show only statistics that correspond to the x-direction (e.g., the mean cloud chord, D_x, and parameter A_x). Note that parameter A_x is inversely proportional to the mean cloud chord D_x (Fig. 4). It is also valid for parameter A_y and the mean cloud chord D_y (not shown). Contrarily to A_x and A_y, the values of parameter A^{up} (upward direction) differ greatly from values of parameter

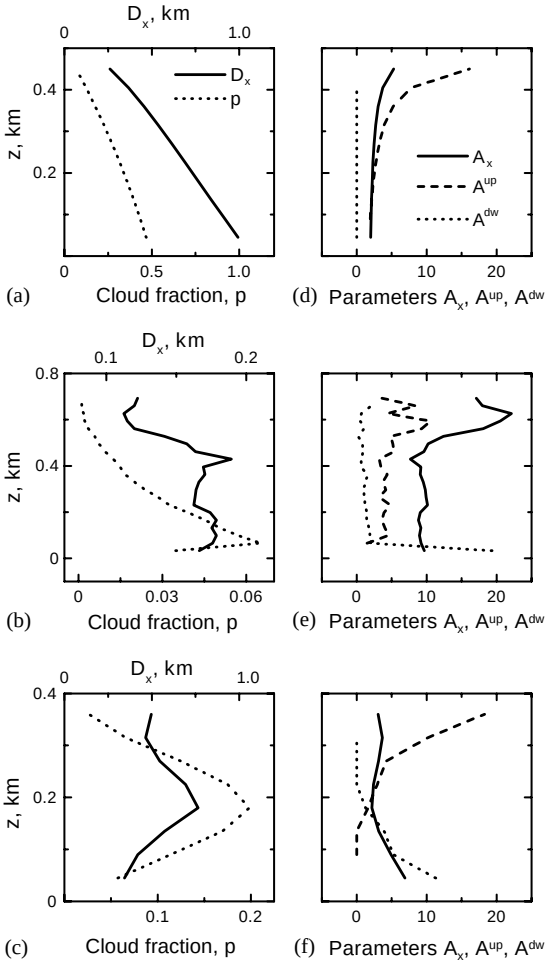

Fig. 4. Left column: the vertical profiles of the cloud fraction, p, and the mean cloud horizontal (x-direction) chord, D_x. Right column: vertical distribution of parameters A_x (x-direction), A^{up} (upward direction) and A^{dw} (downward direction). These bulk cloud statistics were obtained for the Boolean (a,d), LES (b,e) and MISR (c,f) cloud fields.

A^{dw} (downward direction). We are reminded that these parameters describe the statistical relationship between two adjacent cloud layers in the upward and downward directions.

4. Radiative calculation results

4.1. Boolean cloud fields

To estimate the accuracy of the suggested statistical approach we compare the ensemble-averaged radiative properties obtained by two independent methods.

4.1.1. Numerical averaging method

By applying the Boolean stochastic model (see Section 2), realizations of the Markovian cloud field $\kappa(\mathbf{r})$ are simulated for a set of cloud parameters (e.g., nadir-view cloud fraction, the mean horizontal size). In each of these 3D realizations we calculated radiative properties by using a Monte Carlo method (the maximum cross-section approach) and periodical boundary conditions. The ensemble-averaging radiative properties were obtained after appropriate processing. Since the full 3D cloud geometry is used in the radiative calculations, the obtained mean radiative properties are considered as references. To denote these reference radiative properties, we will use subscript "ref".

4.1.2. Analytical averaging method

Approximated equations for the mean radiance, which have been obtained by analytically averaging the stochastic radiative transfer equation, are also used for estimating ensemble-averaged radiative properties. Contrary to the numerical averaging method, another Monte Carlo technique was applied for solving these equations (see Section 2). Since only the bulk cloud statistics (see previous section) are used in the radiative calculations, the mean radiative properties obtained by this method are considered as approximations of the true radiative properties. Note, that using the approximated equations allows one to significantly speed-up (by a factor of 10 to 100) calculations of the ensemble-averaged radiative properties. We will use subscript "app" to denote the approximated radiative properties.

To evaluate the accuracy of the approximated equations (3)–(4), we use the corresponding relative differences (errors)

$$\delta F = \frac{(F_{\mathrm{ref}} - F_{\mathrm{app}})}{F_{\mathrm{ref}}} \times 100\%, \tag{12}$$

where symbol F denotes radiative properties (e.g., mean flux, mean absorption).

The Boolean model and MISR models provided irregular cloud geometry only, but do not provide optical properties. To calculate radiative properties, one needs to know both the geometrical and optical properties of clouds. To introduce significant vertical variability of cloud optical properties, we used different artificial vertical profiles of the extinction coefficient $\sigma(z) = \sigma_k$ and the single scattering albedo $\omega_0(z) = \omega_{0,k}$ with strong vertical gradients. Two types of the vertical profiles were applied. The first type includes vertical profiles of the extinction coefficient $\sigma(z)$ and the single scattering co-albedo, $1 - \omega_0(z)$, that increase with altitude inside a cloud layer (from cloud base to cloud top). Inversely, the second type includes vertical profiles of $\sigma(z)$ and $1 - \omega_0(z)$ that decrease with altitude (from cloud top to cloud base). Since we found that the accuracy of approximated equations is almost independent of the vertical profiles types, below we present results that corresponding to the first type (Fig. 5) only. For the LES field we used values of the extinction coefficient provided by the LES model, but the vertical variability of the single scattering albedo was introduced similar to the Boolean and MISR fields (Fig. 5). To describe scattering by cloud droplets, we applied scattering phase function C.1 [11]. The latter was assumed to be constant and the same for all considered cloud fields. Note that the so-called C.1 model represents cumulus clouds of moderate thickness. For obtaining the reference radiative properties and approximated ones we used the same optical characteristics.

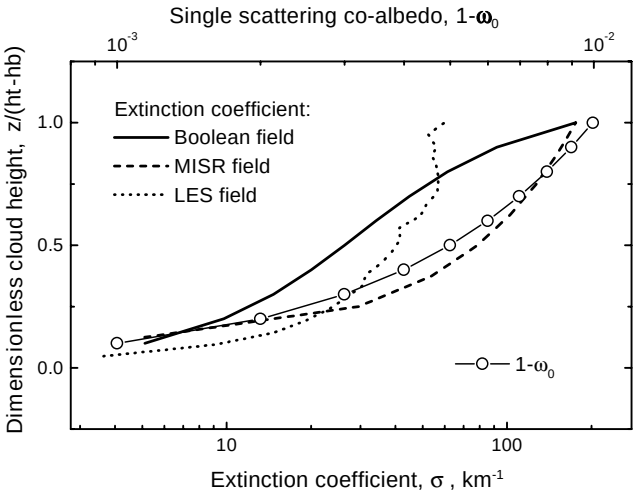

Fig. 5. The vertical profiles of the extinction coefficient and single scattering co-albedo that have been used for radiative calculations. Since the considered cloud fields had different geometrical thickness ($\Delta h = h_t - h_b$), these vertical profiles were shown as functions of dimensionless cloud height.

While the radiative calculations were performed for a set of SZAs, below we demonstrate results for two extreme values SZA = 0 and 70. Since the accuracy of approximated equations may be different for direct (unscattered) and diffuse radiation, we presented corresponding comparisons for both the mean direct radiance, vertical (upward and downward) fluxes and the mean cloud absorption. Here, we considered only the absorption by water droplets. The latter is proportional to the mean order of photon scattering in kth layer. The absorption by the water vapor and other atmospheric gases is a function of the mean photon path length, therefore we include in our analysis the comparison of the photon path length distributions as well.

Two sets of experiments were performed for the Boolean cloud fields. In a cloud field sample, an individual geometry of a cloud is specified as a combination of cylinders with different diameters (e.g. Fig. 2). For the first set of experiments, the centers of these cylinders had the same horizontal coordinates. The cloud statistics for this set are shown in Fig. 4. This set represents an example of the maximum cloud overlap in the downward direction (parameter A^{dw} equals zero). For the second set of experiments, the centers of these cylinders could have the different horizontal coordinates: for each layer these centers were distributed randomly and independently on a horizontal plane. In this case, the cloud fraction $p(z)$, the mean horizontal sizes $D_x(z)$, $D_y(z)$ and the parameters $A_x(z)$, $A_y(z)$ remain the same as in the first experiment (Fig. 4), but the values of other parameters, namely $A^{dw}(z)$ and $A^{up}(z)$, increase radically. This set represents an example of the random cloud overlap in both the upward and downward directions (parameters $A^{dw}(z) \gg 1$, $A^{up}(z) \gg 1$). Hereafter, we will use subscripts "1" and "2" for statistics that correspond to the first and second sets, respectively.

For both sets of experiments cumulative total cloud fraction $p_{total}(z)$ increases in the downward nadir direction (from cloud top to cloud bottom). While the same vertical profiles of the cloud fraction $p(z)$ are used in these two sets of experiments, the rate of this increase is higher for the second set (random cloud overlap). As a result, the value of the nadir-view cloud fraction

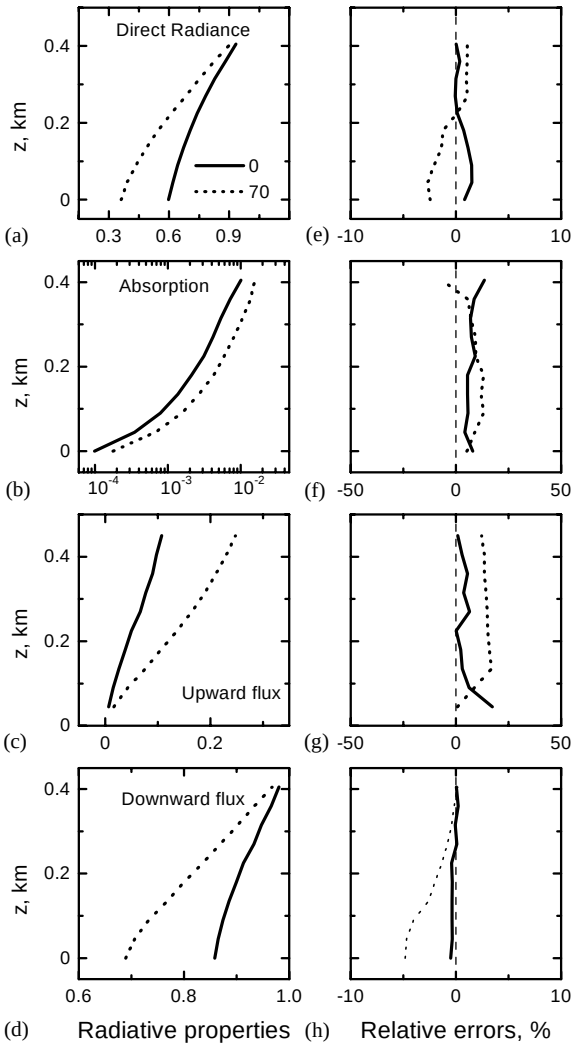

Fig. 6. The ensemble-averaged radiative properties corresponding to the Boolean cloud fields. Left column: the mean vertical profiles of the direct radiance (a), cloud absorption (b), upward flux (c) and downward flux (d) that were obtained by using the numerical averaging method (reference). Right column: the relative differences between the mean vertical profiles that were calculated by using the numerical averaging method and the analytical averaging method (approximation).

$N_{\mathrm{nadir}} = p_{\mathrm{total}}(h_{\mathrm{b}})$ is larger for the second set: $N_{\mathrm{nadir},1} \sim 0.5$, and $N_{\mathrm{nadir},2} \sim 0.9$. For both sets of experiments, 10,000 cloud realizations were simulated to get the mean radiative properties. The mean relative error was about 1% and 10% for the radiative fluxes and their histograms, respectively.

First, we discuss the results obtained for the first set of experiments. Fig. 6 shows the vertical profiles of the mean radiative properties. Recall that all radiative calculations are corresponding to the *unit* solar flux at the top of a cloud layer. As can be seen, for the majority of cases, the relative differences between the exact (the numerical averaging method) and approximated (the analytical

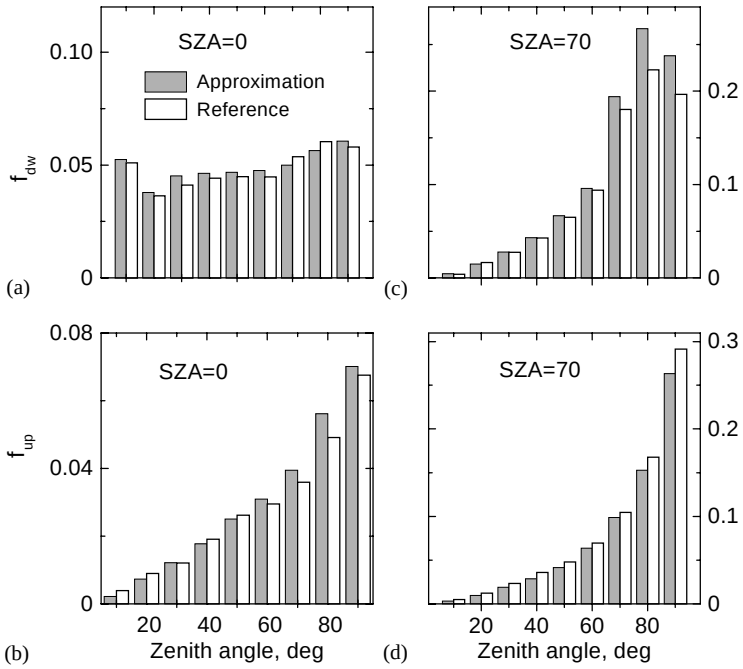

Fig. 7. The Boolean cloud fields. The ensemble-averaged angular distribution histograms of the transmitted (a,c) and reflected (b,d) radiation. These histograms were obtained for two values of SZA by using the numerical averaging method (reference) and the analytical averaging method (approximation).

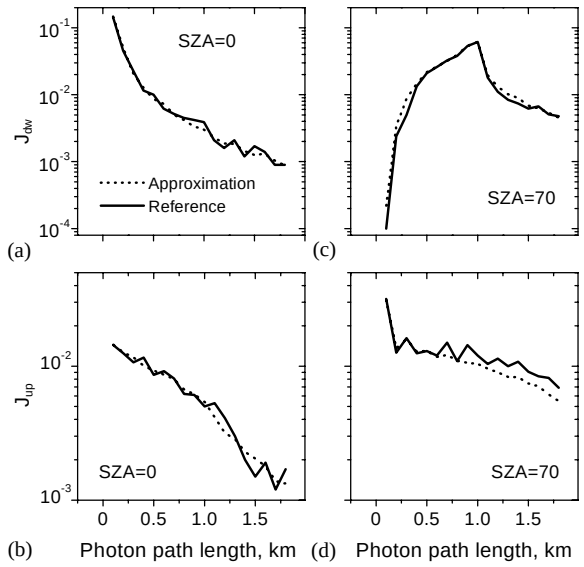

Fig. 8. The Boolean cloud fields. The ensemble-averaged histograms of photon path length distributions in the transmitted (a,c) and reflected (b,d) radiation. These histograms were obtained for two values of SZA by using the numerical averaging method (reference) and the analytical averaging method (approximation).

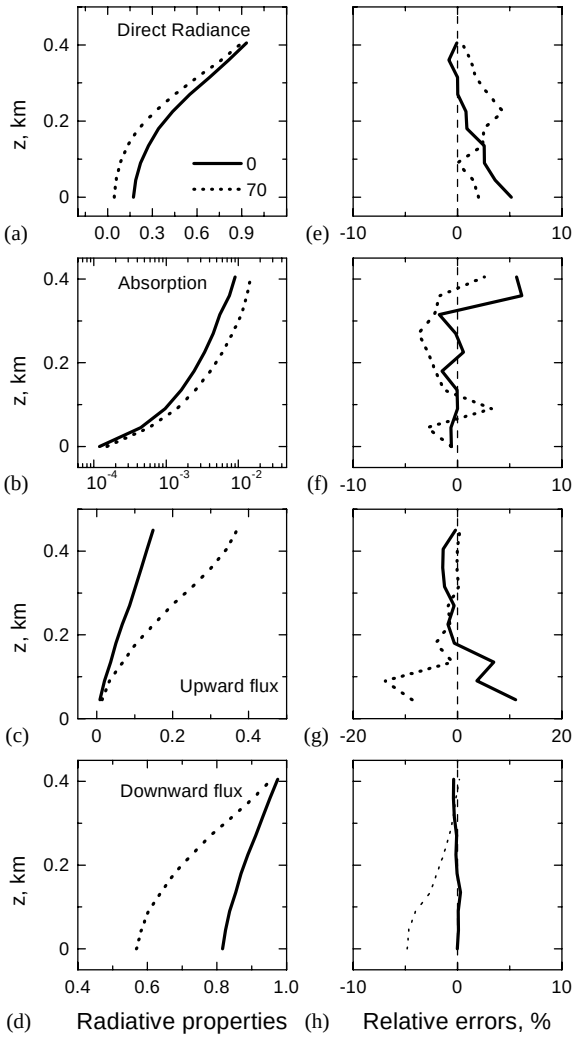

Fig. 9. The same as in Fig. 6, except that these results correspond to the *random* cloud overlap (parameters $A^{dw}(z) \gg 1$, $A^{up}(z) \gg 1$).

averaging method) radiative properties do not exceed 10%. A similar good agreement is also observed for the angular distribution histograms (Fig. 7) and the histograms of photon path length distributions (Fig. 8). Note, that for transmitted photons the path length l means the path length minus the cloud layer geometrical thickness.

Next, we discuss the second set of experiments shown in Figs. 9–11. As mentioned above, the cumulative total cloud fraction $p_{total}(z)$ increases faster for the random cloud overlap (the second set) than for the maximum cloud overlap (the first set). Since the mean direct radiance $\langle S(z)\rangle$ is proportional to $1 - p_{total}(z)$, then $\langle S_2(z)\rangle$ decreases more significantly inside the cloud layer (from cloud top to cloud bottom) for the random cloud overlap than for the maximum cloud overlap. As a result, at the cloud base $\langle S_2(0)\rangle$ is considerably less than $\langle S_1(0)\rangle$ (i.e., cf. Fig. 6a to Fig. 9a).

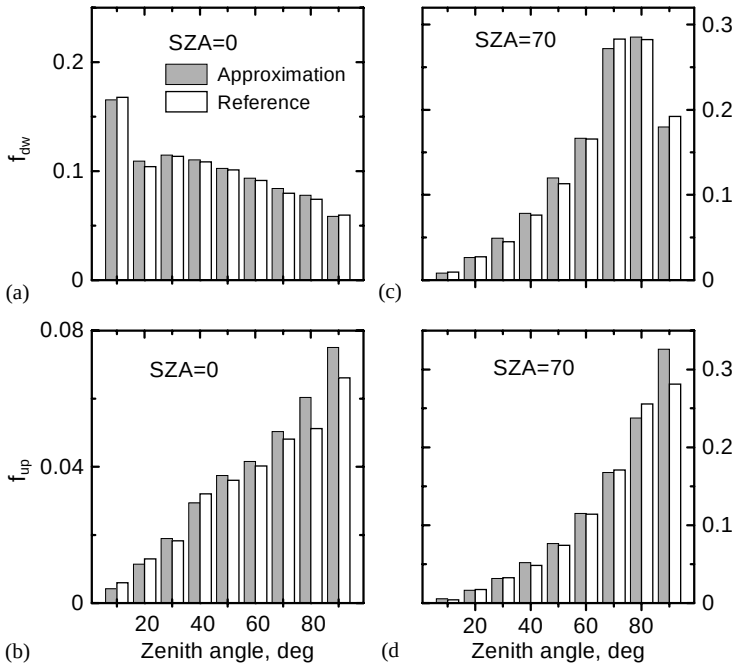

Fig. 10. The same as in Fig. 7, except that these results correspond to the *random* cloud overlap (parameters $A^{dw}(z) \gg 1$, $A^{up}(z) \gg 1$).

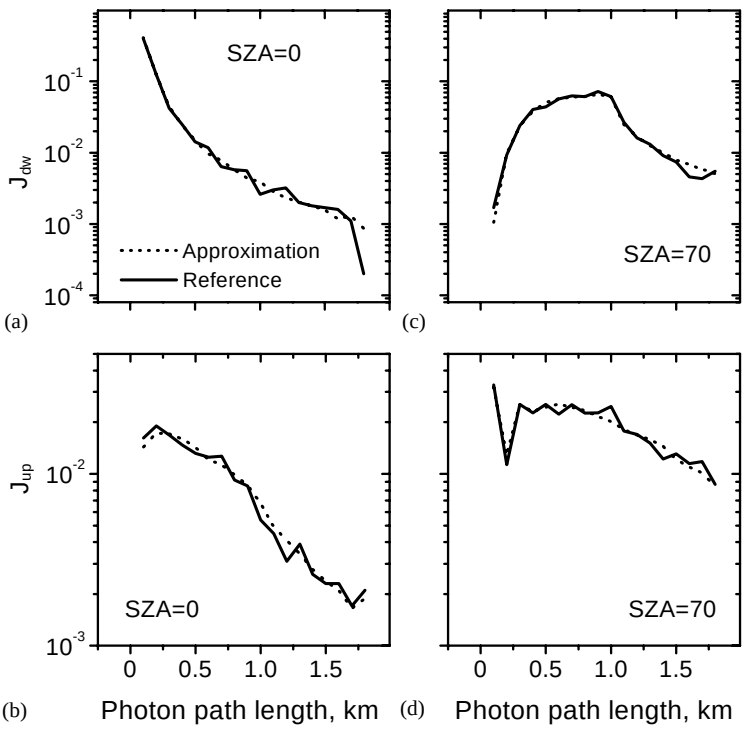

Fig. 11. The same as in Fig. 8, except that these results correspond to the *random* cloud overlap (parameters $A^{dw}(z) \gg 1$, $A^{up}(z) \gg 1$).

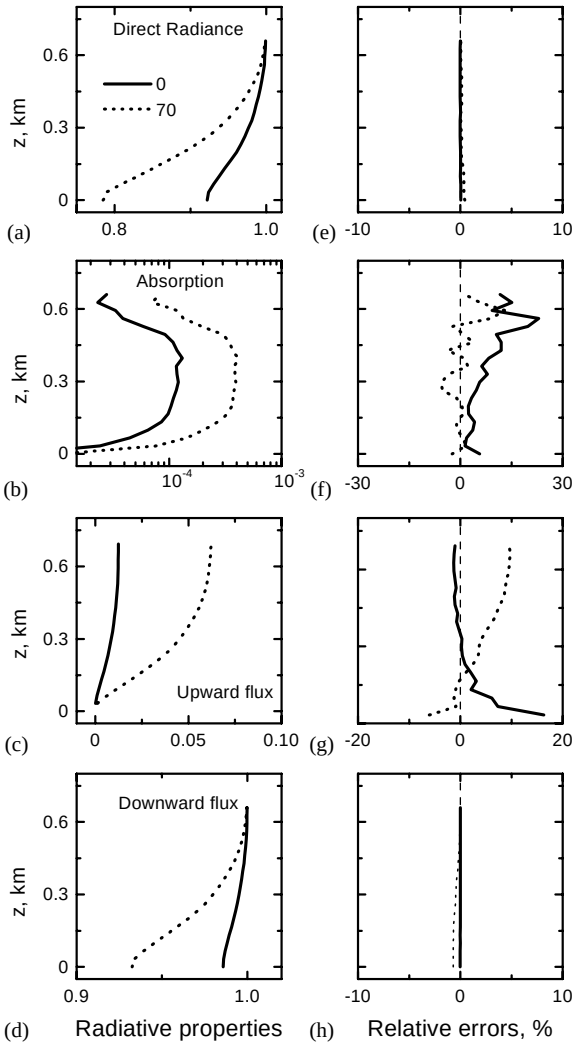

Fig. 12. The domain-averaged radiative properties corresponding to the LES cloud fields. Left column: the mean vertical profiles of the direct radiance (a), cloud absorption (b), upward flux (c) and downward flux (d) that were obtained by using full 3D cloud structure (reference). Right column: the relative differences between the mean vertical profiles that were calculated by using full 3D cloud structure (reference) and the bulk cloud statistics (approximation).

The fraction of the scattered and absorbed radiation in a whole cloud layer is $1-\langle S(0)\rangle$; therefore, for the random cloud overlap, this fraction is substantially larger. For example, the mean upward flux $\langle F_{2,\mathrm{up}}(z)\rangle$ is nearly twice as large as $\langle F_{1,\mathrm{up}}(z)\rangle$ (Figs. 6c,9c). Similar quantitative differences are observed for corresponding the angular distribution histograms (Figs. 7,10), and the histograms of photon path length distributions (Figs. 8,11). Note, that for given cloud fields, the mean vertical profiles of absorption depend weakly on the cloud overlap. Here, we considered absorption by water droplets only, and the latter is proportional to the mean order of photon scattering in the kth

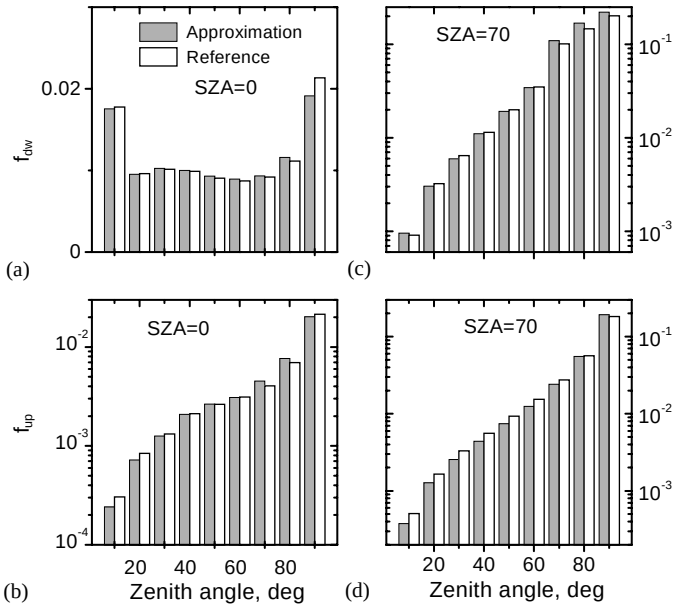

Fig. 13. The LES cloud field. The domain-averaged angular distribution histograms of the transmitted (a,c) and reflected (b,d) radiation. These histograms were obtained for two values of SZA by using full 3D cloud structure (reference) and the bulk cloud statistics (approximation).

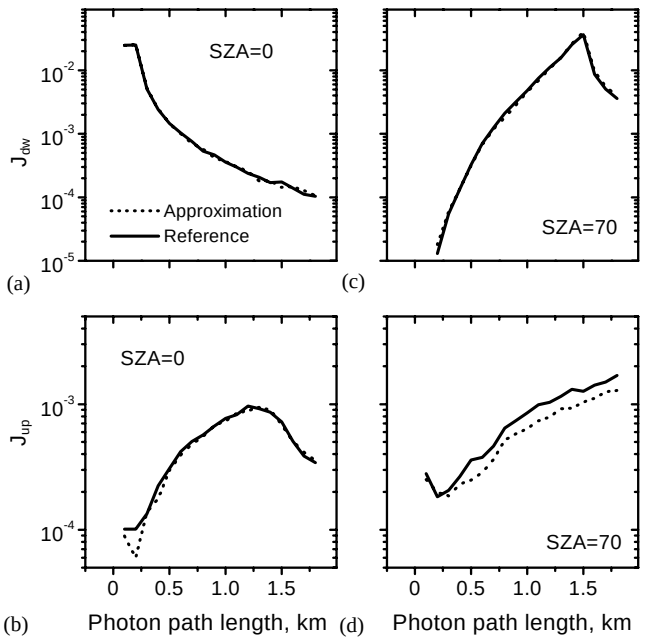

Fig. 14. The LES cloud field. The domain-averaged histograms of photon path length distributions in the transmitted (a,c) and reflected (b,d) radiation. These histograms were obtained for two values of SZA by using full 3D cloud structure (reference) and the bulk cloud statistics (approximation).

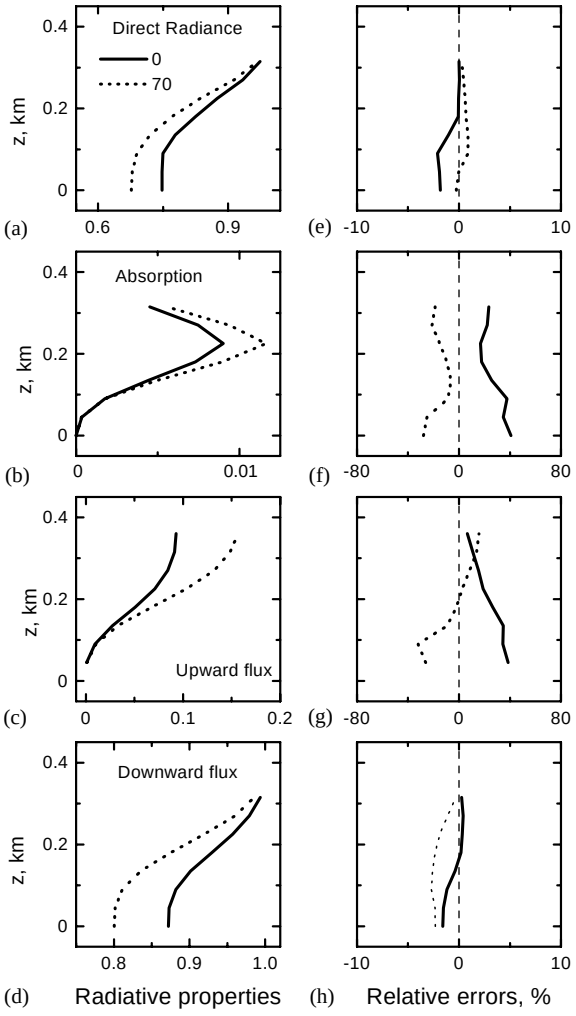

Fig. 15. The same as in Fig. 12, except that these results correspond to the MISR cloud field.

sublayer (for given $\omega_{0,k}$). Therefore, it may be suggested that the cloud overlap affects only slightly the mean values of the scattering multiplicity. As for the first set of experiments, the suggested statistical approach performs well for the second one (Figs. 9–11). Note these good agreements were obtained for *ensemble-averaged* radiative properties and *artificial* Markovian cloud fields. Therefore, the question arises: How well will the suggested statistical approach perform for a *single* realization of *real* cloud fields?

In other words, is the suggested approach robust?

4.2. LES and MISR cloud fields

Eqs. (3) and (4) for the mean radiance have been obtained by averaging over a set of cloud realizations (ensemble-averaged statistics). This makes it necessary to study a large group of such

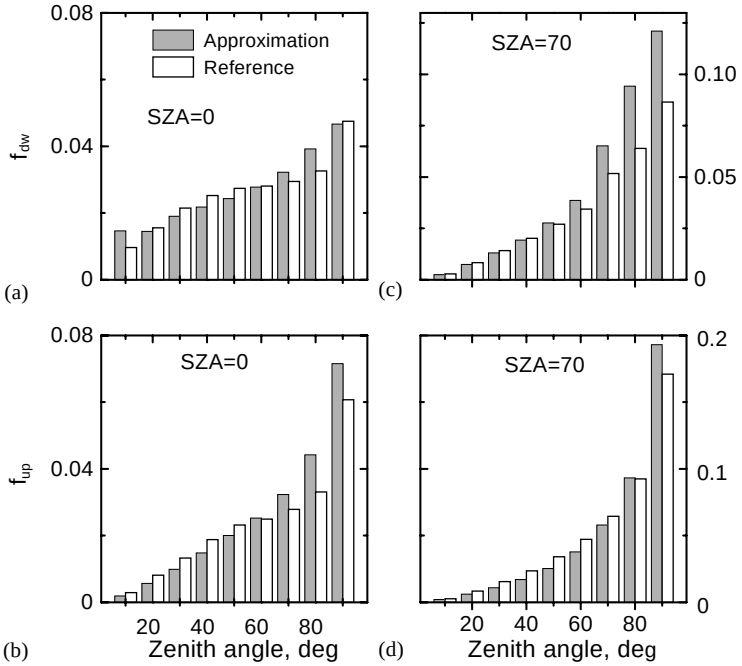

Fig. 16. The same as in Fig. 13, except that these results correspond to the MISR cloud field.

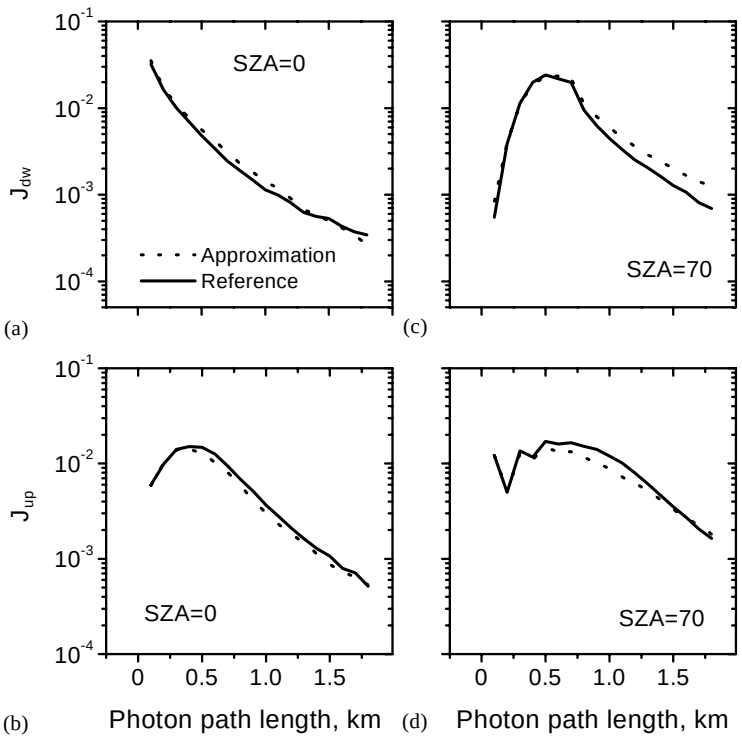

Fig. 17. The same as in Fig. 14, except that these results correspond to the MISR cloud field.

realizations, which as a rule the researcher does not have. To experimentally determine these statistical properties, one can apply the generally used *ergotic* assumption. In this case, the sought characteristics can be obtained from single, sufficiently large realization (domain-averaged statistics). In other words, it is assumed that the domain-averaged statistics and the ensemble-averaged statistics are interchangeable. Note, the ergotic assumption is valid for Markovian random fields.

In this section, the validation analysis is similar to that described above (Section 3.1), except that *domain-averaged* statistics were taken into account only. The bulk cloud statistics (Fig. 4) were obtained from the single cloud realizations of the MISR and LES cloud fields (Fig. 1). It is worth noting that (i) the LES cloud field contains a lot of small clouds (cloud horizontal size $D \leqslant 1$ km), and (ii) the MISR is composed of a few large clouds ($D \sim 5$ km) surrounded by small clouds. Similar to the Boolean cloud field, the domain-averaged radiative properties were calculated by two independent methods. The full 3D cloud geometry was used in the first method (reference), and only the bulk cloud statistics (Fig. 4) were applied for the second method (approximation).

Results of the radiative calculations are shown in Figs. 12–17. For the LES cloud field there is reasonable agreement between the exact and approximated results (Figs. 12–14): while the maximum relative differences are about 25%, for the majority cases the accuracy of approximated radiative calculations do not exceed 10%. The histograms of (i) the angular distribution and (ii) the photon path length distribution in transmitted and reflected radiation, which have been obtained by exact and approximated methods, agree qualitatively and quantitatively (Figs. 13,14). Similar results were obtained for the MISR cloud field (Figs. 15–17), except the maximum relative differences can be as large as 40%. Note, these large relative errors are associated with small absolute values of the mean upward flux and mean absorption in the bottom part of cloud layer. The relative errors of the mean upward flux at the cloud top (mean albedo) and the mean total absorption (from cloud top to cloud bottom) are less. Moreover, the approximated radiative calculations underestimate these radiative properties for SZA $= 0$ (Sun is in zenith), and inversely, overestimate them for SZA $= 70$ (Sun is close to the horizon); for other intermediate SZA values these relative differences are less as well.

The differences between the exact and approximated domain-averaging results can be determined by two factors. First, the Markovian approximation can be inappropriate for a given 3D cloud realization (cloud sample). Second, the sample size can be insufficiently large for obtaining the cloud statistics. Obviously, the sample size of a given realization is a function of a cloud type (e.g., mean horizontal size D, and the nadir-view cloud fraction N_{nadir}). Here, we can only say that, for small ($D \sim 1$ km) marine cumulus clouds, it should be $\sim 10 \times 10$ km^2 and larger. In other words, a given cloud sample should contain many clouds.

5. Conclusion

Our two-part paper is designed to introduce a statistical approach for the solar radiative calculations in multilayer broken clouds. In Part I the equations for the mean solar radiance were derived by using the analytical averaging method. In this paper (Part II), we estimated the accuracy and robustness of these equations. The validation analysis of the suggested statistical approach was performed by using 3D broken cloud fields produced by (i) Boolean stochastic model, (ii) LES models and (iii) MISR cloud retrieval. The LES and MISR cloud fields represent a marine boundary layer broken clouds at the ARM TWP site.

The accuracy of the obtained equations was evaluated by comparing the *ensemble-averaged* radiative properties that were obtained by the numerical averaging method (reference) and the analytical averaging method (approximation). The Boolean stochastic model was applied to simulate ensemble of realizations of 3D broken cloud with given vertical and horizontal structure. It was demonstrated that the suggested approach allows one to estimate the ensemble-averaged vertical profiles of cloud absorption and upward/downward radiative fluxes with reasonable accuracy ($\sim$10%). The angular distribution histograms and the photon path length distributions of the mean albedo and transmittance, which have been obtained by exact and approximated methods, agree qualitatively and quantitatively.

The robustness of these equations was estimated by comparing the *domain-averaged* radiative properties obtained by using (i) the full 3D cloud structure of a given cloud sample (reference) and (ii) the bulk cloud statistics (approximation). Single realizations of the LES (domain size 10×10 km^2) and MISR (domain size $\sim 30 \times 30$ km^2) cloud fields were applied for this robustness analysis. We found the suggested approach allows one to estimate the *domain*-averaged radiative properties quite accurately, and the errors of approximated radiative calculations depend on cloud type. For the LES cloud field, there is satisfactory agreement ($\sim$15%) between the approximated and reference radiative properties. For the MISR cloud field, a similar accuracy ($\sim$15%) was obtained for the domain-averaged albedo and transmittance. The maximum relative errors can be more than two times larger for the vertical profiles of the mean upward flux and cloud absorption in the bottom part of the cloud field; these large relative errors are associated with small absolute values of the radiative properties.

The validation tests indicate that the suggested statistically inhomogeneous Markovian model is capable of capturing the mean radiative properties and their specific features (e.g. the vertical and angular distribution of the mean vertical fluxes) for marine low-level cumulus clouds. The accuracy of the approximated radiative calculations associated with different cloud types and the sample size requires further investigations.

Acknowledgements

This work was supported by the Office of Biological and Environmental Research of the U.S. Department of Energy as part of the ARM Program and by NASA under contract (no. 121164 with NASA/Jet Propulsion Laboratory (JPL). We are grateful to Ms. N. Burleigh for her help to prepare the paper.

References

[1] Stephens GL. Radiative transfer through arbitrarily shaped optical media. Part II: group theory and simple closures. J Atmos Sci 1988;45:1837–48.

[2] Stephens GL, Gabriel PM, Tsay SC. Statistical radiative transport in one-dimensional media and its application to the terrestrial atmosphere. Transport Theor Statist Phys 1991;20:139–75.

[3] Barker HW, Stephens GL, Fu Q. The sensitivity of domain-averaged solar fluxes to assumptions about cloud geometry. Q J R Meteorol Soc 1999;125:2127–52.

[4] Geleyn JF, Hollingsworth A. An economical analytical method for the computation of the interaction between scattering and line absorption of radiation. Contrib Atmos Phys 1979;52:1–16.

[5] Kassianov EI. Stochastic radiative transfer in multilayer broken clouds. Part I: Markovian approach. JQSRT 2003;77:373–93.
[6] Marchuk G, Mikhailov G, Nazaraliev M, Darbinjan R, Kargin B, Elepov B. The Monte Carlo methods in atmospheric optics. New York: Springer, 1980.
[7] Stoyan D, Kendall WS, Mecke J. Stochastic geometry and its applications. Chichester: Wiley, 1995. 389pp.
[8] Kassianov EI, Ackerman TP, Marchand RT, Ovtchinnikov M. Satellite multi-angle cumulus geometry retrieval. J Geophys Res 2002, submitted for publication.
[9] Benner TC, Curry JA. Characteristics of small tropical cumulus clouds and their impact on the environment. J Geophys Res 1998;103:28,753–67.
[10] Clothiaux EE, Moran KP, Martner BE, Ackerman TP, Mace GG, Uttal T, Mather JH, Widener KB, Miller MA, Rodriguez DJ. The Atmospheric Radiation Measurement Program cloud radars: operational modes. J Atmos Sci 1999;56:819–27.
[11] Deirmendjian D. Electromagnetic radiation scattering by spherical polydisperse particles. New York: Elsevier, 1969. 290pp.